Journal of Hydrology 374 (2009) 30–42

Contents lists available at ScienceDirect

Journal of Hydrology

journal homepage: www.elsevier.com/locate/jhydrol

Infiltration and deep flow over sloping surfaces: Comparison of numerical and experimental results

Emily T. Essig [a], Corrado Corradini [b], Renato Morbidelli [b], Rao S. Govindaraju [a,*]

[a] School of Civil Engineering, Purdue University, West Lafayette, IN 47906, USA
[b] Dept. of Civil and Environmental Engineering, University of Perugia, via G. Duranti 93, 06125 Perugia, Italy

ARTICLE INFO

Article history:
Received 16 October 2008
Received in revised form 13 May 2009
Accepted 23 May 2009

This manuscript was handled by P. Baveye, Editor-in-Chief, with the assistance of Juan V. Giraldez, Associate Editor

Keywords:
Infiltration
Saturated–unsaturated flow model
Sharp-front model
Hydrus
Numerical solutions

SUMMARY

Infiltration and deep flow on sloping surfaces were studied by combining controlled laboratory experiments with mathematical models. Experimental variables included soil types, rainfall intensities, and surface slopes. Preliminary analyses of the data indicated that increased slope has a positive influence on surface flow, and that this influence increases relatively with decreasing rainfall rate. However, current theories could not adequately explain the observed behavior of deep and surface flows for varying slopes. Three mathematical models of varying complexity were employed to supplement the experimental results. These models were (i) the 2-D Hydrus numerical model, (ii) numerical solution of 1-D saturated–unsaturated flow equation on sloping surfaces, and (iii) a simplified 1-D sharp-front model for sloping surfaces. For the latter two models, a surface flow component based on the kinematic wave approximation for shallow flows was externally coupled to the subsurface flows to route water over the soil surface. For each soil, one experiment at the lowest slope and rainfall rate was utilized for estimation of model parameters that could not be measured independently, while all the other results were used for model corroboration. The Hydrus model indicated that a 1-D analysis would be adequate as the water front moves essentially parallel to the slope. To account for the influence of slope and soil-type on experimental results, an effective saturated conductivity was proposed. Model results were found to be in reasonable agreement with observations of surface flow, deep flow, and water contents in the soil profile with the use of the proposed effective saturated conductivity. Limitations on the applicability of the sharp-front model in this context were discussed.

Introduction

Infiltration plays a pivotal role in the hydrologic cycle by partitioning rainfall into surface and subsurface components. Soil hydraulic properties, rainfall rate, and the initial (antecedent) water content of the soil are some of the factors that govern infiltration into the soil. One factor that has received little attention is the effect of slope on the relationship between runoff and infiltration.

Past studies have provided conflicting conclusions as to whether infiltration and deep flow increase or decrease with increasing slope. Among the early studies on infiltration on sloping surfaces, Poesen (1984) observed a decrease in runoff with an increase in slope for soils susceptible to surface crust formation (increased infiltration for increased slopes). Poesen's experiments showed that runoff coefficients were higher for a 2% slope than a 15% slope, and that the mean percolation coefficient was lower for the 2% than 15% slope. The results indicated a positive relationship between slope and infiltration rate, especially for soils with water content at field capacity or greater. Poesen attributed the decreased runoff to either a thinner soil crust or increased rill erosion on the steeper slopes. It was concluded that surface sealing is inversely related to slope, so steeper slopes would have a thinner compacted soil layer than flatter slopes, and would be more prone to infiltration. Steeper slopes also erode more quickly, and increased erosion forms deeper rills, and therefore increases the surface area over which infiltration can occur. Thus, if erosion and surface sealing do not occur, then slope would not be expected to affect infiltration rate. Poesen did not go into detail on non-filled soils, or to soils that are resistant to soil crust formation, but believes that infiltration would decrease with slope for these soils because ponding and small depressions are not present on sloped surfaces as they are on flat surfaces. Therefore, further studies are needed on non-surface sealing soils with no depression storage-related erosion to isolate the effects of slope on infiltration behavior.

Philip (1991) conducted a mathematical study on the effects of surface slope on the dynamics of infiltration. By applying Richards'

* Corresponding author. Tel.: +1 765 496 3402; fax: +1 765 494 0395.
E-mail addresses: EESSIG@PURDUE.EDU (E.T. Essig), CORRADO@UNIPG.IT (C. Corradini), RENATO@UNIPG.IT (R. Morbidelli), GOVIND@PURDUE.EDU (R.S. Govindaraju).

0022-1694/$ - see front matter © 2009 Elsevier B.V. All rights reserved.
doi:10.1016/j.jhydrol.2009.05.017

equation to a sloping surface, he showed that infiltration decreases as slope increases by a factor of $\cos\gamma$, where γ is the angle of the surface slope with the horizontal. The theory assumes that initial water content is uniform and that the flat surface has infinite extent. It does not take into account initial soil conditions of hydrostatic equilibrium (variable water content), nor is it directly applicable to experiments where wall effects and bottom boundary condition are important.

Richards' equation is highly nonlinear, and does not admit analytical solutions. A simplified sharp-front model (Green and Ampt, 1911; Mein and Larson, 1973) is often used to estimate infiltration over flat surfaces. Chen and Young (2006) extended the Green–Ampt approach to sloping surfaces. Numerical results elucidated the role of gravity and capillary forces, rainfall intensities, and slope angle on infiltration-both at small and large times. For very large times, large rainfall intensities, or slopes less than 10°, the differences became insignificant. Because the effective slope length (area) increased for the steeper experiments, capillary forces alone would cause an apparent increased infiltration rate, as they are independent of slope angle for homogenous and isotropic soils. The dominating gravitational effects would be reduced by a factor of $\cos\gamma$, but the effect would cancel by increasing the slope length, and the slope effect would disappear with time. The study focused on infiltration, and did not describe how the moisture front moves in the soil column, or how redistribution occurs after rain stops. Both Philip (1991) and Chen and Young (2006) assumed infinitely deep soils, and their analyses are not valid for a finite laboratory soil box study.

Smith and Woolhiser (1971) focused on overland flow over sloping infiltrating surfaces. The kinematic wave approximation was used to describe unsteady overland flow and was linked dynamically to an infiltration model by using boundary conditions at the soil surface. The model was tested by comparisons to data from a laboratory experiment and a field plot. The study found good agreement between measured and predicted hydrographs, but differences in the recession limb were noted. The influence of slope was not examined in this study.

Dagan and Bresler (1983) derived models of infiltration and redistribution for unsaturated flow in spatially variable fields using a sharp-front approximation. They combined Richards' equation with hydraulic properties described by the Brooks–Corey model to solve for vertical flow in a field whose saturated conductivity varies in space according to a log-normal distribution. In determining the applicability of sharp-front models, Govindaraju et al. (1992, 1996) determined that the approximate (sharp-front) model leads to reasonably accurate values of expected flow variables over the entire field because model errors cancel in the averaging process, and local-scale dispersion of the water front is much smaller than the dispersion from field-scale variability in hydraulic properties. However, the models in these studies were restricted to non-sloping surfaces, and resulting surface flows were not modeled.

A preliminary analysis of laboratory experiments concerning the hydrological response of a slope to synthetic rainfall conducted at the University of Perugia, Italy, showed that observations deviated from theoretical expectations. These controlled laboratory experiments suggest that a better understanding of the role of surface slope is needed to improve our ability to accurately calculate the surface runoff and deep flow hydrographs on sloping surfaces. The main goal of this study is to shed some light on these discrepancies using numerical solutions, and to propose a new definition of effective hydraulic conductivity that accounts for the influence of slope on infiltration process. Section "Laboratory experiments and preliminary analysis" describes the laboratory experiments and highlights these discrepancies. Section "Mathematical development and numerical models" presents the mathematical development, including that of the sharp-front approximation on sloping surfaces which is additional new material in this paper. Section "Comparisons of numerical results and observations" presents comparisons of experimental and numerical results, while Section "Summarizing remarks" summarizes the work and states the conclusions from this study.

Laboratory experiments and preliminary analysis

A soil box 152 cm long, 122 cm wide, and 78 cm deep with adjustable slope (from 1° to 15°) was utilized in the laboratory experiments. The sides are impermeable and transparent. The top and bottom surfaces are open to the atmosphere.

For the experiments of interest to this study, surface runoff and deep flow were measured using calibrated tipping-bucket sensors at the downstream end of the soil surface and the bottom. An overhead pressurized water sprinkler system was adjusted to generate specific rainfall rates. The soil was uniformly packed to a depth of 67 cm in the box. A 7 cm gravel layer separated by a textile mesh below the soil speeds the drainage of the percolated water from the soil (details in Morbidelli et al., 2008; Essig, 2008).

Three different soils types were used in three separate sets of experiments. The set with the first soil type (Soil-1) comprised of 24 experiments ranging in slopes from 1° to 15° and average rainfall rates ranging from 10 mm/h to 20 mm/h. The set with the second soil type (Soil-2) comprised of eight experiments with slopes ranging from 1° to 15° and average rainfall rates of 10 and 15 mm/h. Only for Soil-2, the water content profile was continuously monitored using the TDR method (TRASE-BE, Soil Moisture Equipment Corp., Goleta, CA). Two vertical profiles were observed, with measurements made at 10, 20, 30, 45 and 60 cm depths for each profile. Each probe provided an average measurement of the volumetric water content at the corresponding depth. The set with the third soil type (Soil-3) comprised of 18 experiments where slopes ranged from 1° to 10° and average rainfall rates of 20–30 mm/h were applied.

The United States Department of Agriculture (USDA) classifies soils based on particle size. Table 1 summarizes the distribution of soil particles based on the USDA classification for Soil-1, Soil-2 and Soil-3. Bin sizes were interpolated from the soil grain size distribution. As shown in Table 1, Soil-1 is mostly silt and clay, Soil-2 is primarily sand and silt, and Soil-3 is mostly sand with silt as well, but has the greatest fraction with particles sizes greater than 2 mm. We label Soil-1 as a clay loam, Soil-2 a loam, and Soil-3 a sandy loam (when grouping the gravel with sand and accounting for the larger gravel fraction in Soil-3).

For each experiment, rainfall was applied to achieve soil saturation throughout the box. There was a short time period between

Table 1
Size classification for the three experimental soils.

Soil type	Size (mm)	Percent of Soil-1	Percent of Soil-2	Percent of Soil-3
Gravel	>2	0.74	1.22	4.00
Sand	.05–2	25.12	40.99	37.97
Silt	.002–.05	41.91	34.95	35.11
Clay	<.002	32.23	22.84	22.92

bringing the soil to saturation and the beginning of each experiment. There was no deep flow at the start of the experiment, so the initial water content could be approximated by a hydrostatic pressure distribution. Each experiment run composed of 8 h of applied rainfall. Surface runoff and deep flow were collected for up to 24 h using calibrated tipping-bucket sensors with variable collection intervals. A detailed description of the laboratory experimental setup can be obtained from Morbidelli et al. (2008).

A summary of the observed results for Soil-1, Soil-2 and Soil-3 are included in Tables 2–4, respectively. As expected, it was observed that the time to ponding increased as rainfall intensities decreased. Surface flowrate (normalized by the average rainfall rate) versus time were used to compare runoff rates for different slopes, soil types, and rainfall rates. Although the rainfall was set to a specific reference rainfall, the actual average rainfall rate deviated slightly from the reference rainfall. Fig. 1 shows surface and deep flow hydrographs for Soil-1 with a reference rainfall of 10 mm/h. For Soil-1, the slope has a positive influence on the steady state surface flow, i.e. greater slopes show larger normalized surface flow and smaller normalized deep flow.

Based on kinematic wave theory, the time of concentration for Soil-1 should be under 1 h. However, a longer than expected receding limb of surface flow was observed after the rainfall was turned off (Fig. 1). This tail is more prominent for steeper slopes. This tailing surface runoff is less noticeable for Soil-2 (Fig. 2), and is barely present for the Soil-3 (Fig. 3) for all slopes considered here. The normalized graphs of Soil-1 suggest the presence of soil water outflow near saturation (i.e. a seepage face), but this is not as apparent for Soil-2 and Soil-3 for the 10 and 20 mm/h reference rainfalls, respectively.

Conceptually, one would expect that that the normalized steady deep flow should only vary with $\cos\gamma$ (Chow et al., 1988; Philip, 1991; Chen and Young, 2006), but our results did not conform to this expectation because the steady deep flow normalized by $\cos\gamma$ versus the slope did not result in a horizontal line in Fig. 4. The deep flow decreased by more than a $\cos\gamma$ factor. Analysis of the observed results indicates that relationships between rainfall and surface runoff (and deep flow) are being influenced by other factors. The following factors could be hypothesized as playing a role:

- The walls of the sand box enforce a condition of zero flux normal to the boundary. This may be distorting the flow pattern sufficiently so that the flow is strongly influenced by wall effects.
- A longer recession tail, especially for the steeper slopes in Soil-1 suggests the presence of return flow from saturated areas. This return flow, if it exists, would be more prominent for steep slopes and for fine-textured soils.

Table 2
Summary of observed data for Soil-1.

Experiment number	Slope (°)	Average rainfall (mm/h)	Time to ponding (h, min)	Steady surface flow (mm/h)
Reference rainfall rate 10 mm/h				
1	1	9.86	0.58	6.73
3	5	9.74	0.52	7.69
5	10	10.07	0.39	8.83
7	15	9.85	0.40	8.94
9	10	9.11	0.50	7.73
11	15	8.85	0.43	8.37
13	5	9.55	0.50	7.09
15	1	9.49	0.49	6.50
Reference rainfall rate 15 mm/h				
2	1	15.02	0.27	12.44
4	5	15.16	0.23	13.11
6	10	14.62	0.27	13.1
8	15	14.3	0.24	13.53
10	10	14.56	0.25	13.32
12	15	13.18	0.23	12.76
14	5	13.81	0.28	11.49
16	1	14.74	0.25	11.89
Reference rainfall rate 20 mm/h				
17	1	20.84	0.19	18.12
18	1	21.5	0.15	19.11
19	5	20.49	0.15	18.25
20	5	20.28	0.16	18.17
21	10	20.04	0.14	18.25
22	10	20.02	0.13	18.23
23	15	20.49	0.13	19.36
24	15	19.84	0.12	19.07

Table 3
Summary of observed data for Soil-2.

Experiment number	Slope (°)	Average rainfall (mm/h)	Time to ponding (h, min)	Steady surface flow (mm/h)
Reference rainfall rate 10 mm/h				
1	1	9.81	0.33	6.73
3	5	9.77	0.23	7.04
5	10	9.91	0.22	7.43
7	15	9.63	0.09	8.11
Reference rainfall rate 15 mm/h				
2	1	15.69	0.18	12.7
4	5	15.92	0.14	13.38
6	10	15.02	0.1	12.75
8	15	13.9	0.04	12.44

Table 4
Summary of observed data for Soil-3.

Experiment number	Slope (°)	Average rainfall (mm/h)	Time to ponding (h, min)	Steady surface flow (mm/h)
Reference rainfall rate 20 mm/h				
13	1	18.08	0.43	8.02
14	1	19.32	0.37	8.76
15	5	18.82	0.30	8.53
16	5	18.29	0.30	8.66
17	10	18.61	0.14	9.07
18	10	18.36	0.17	8.9
Reference rainfall rate 25 mm/h				
1	1	25.49	0.17	15.39
2	1	25.95	0.15	15.74
5	5	25.86	0.17	15.45
6	5	25.83	0.16	15.5
9	10	25.82	0.1	15.73
10	10	25.87	0.1	16.33
Reference rainfall rate 30 mm/h				
3	1	31.43	0.11	21.02
4	1	32.4	0.12	22.19
7	5	32.12	0.08	21.91
8	5	32.31	0.1	22.06
11	10	30.37	0.15	20.55
12	10	31.34	0.06	21.29

- The infiltration of water moving on the soil surface is different from the case of infiltration over a flat surface where the ponded water has no momentum in the direction tangential to the slope.

To investigate these hypotheses, numerical models were used to interpolate and interpret the experimental results.

Mathematical development and numerical models

Three different numerical models were used to analyze the laboratory experiments: (i) the Hydrus numerical model, (ii) numerical solution of 1-D saturated–unsaturated flow equation on sloping surfaces, and (iii) a simplified 1-D sharp-front model for sloping surfaces. The last two models were combined with a kinematic approximation to simulate surface flow hydrographs and to provide a time-space varying boundary condition for the soil surface. These models are described below.

Hydrus model

Hydrus is a software package for simulating water, heat and solute movement in 2-D or 3-D variably saturated media (Simunek et al., 2007a,b). The program uses the finite element method to obtain a numerical solution to Richards' equation for unsaturated water flow. The numerical model does not accommodate surface flow, but it serves two important purposes. First, it helps to investigate two of the possibilities listed before, i.e. whether wall effects are prominent, and if there is sufficient build up of pressure within the soil profile to support an argument for return flow. Secondly, it allows us to assess whether a 1-D representation for subsurface flow process is justified, thus paving the way for the second and third simplified model approaches. Hydrus also computes the water fluxes leaving the top and bottom boundary layer, and the predominant water movement direction within the soil column. Soil-1, Soil-2, and Soil-3 were simulated in 2-D at the highest

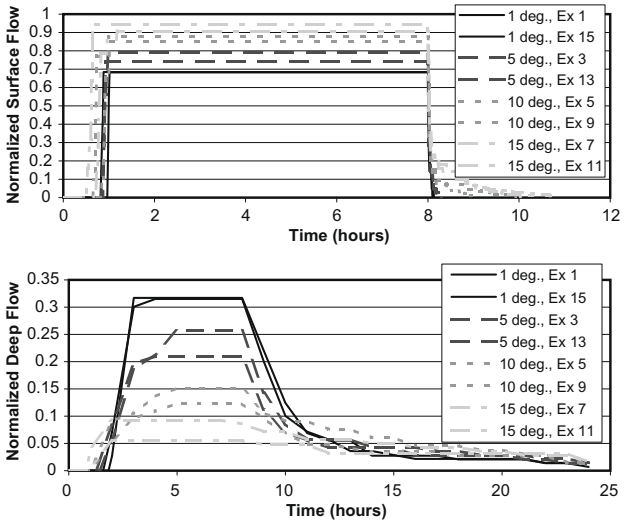

Fig. 1. Normalized surface and deep flow for Soil-1 under reference rainfall = 10 mm/h. The flow was normalized by the average rainfall rate. See Table 2 for average rainfall rates.

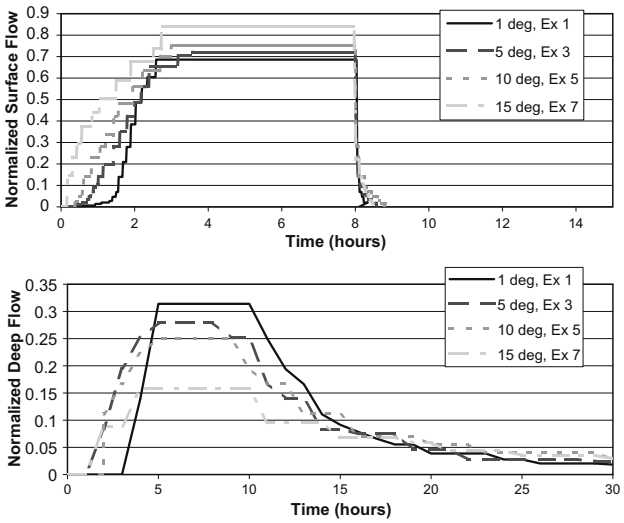

Fig. 2. Normalized surface and deep flow for Soil-2 under reference rainfall = 10 mm/h. The flow was normalized by the average rainfall rate. See Table 3 for average rainfall rates.

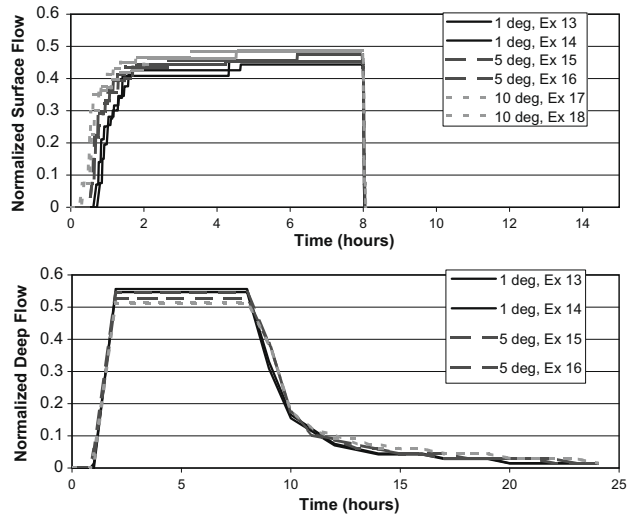

Fig. 3. Normalized surface and deep flow for Soil-3 under reference rainfall = 20 mm/h. The flow was normalized by the average rainfall rate. See Table 4 for average rainfall rates.

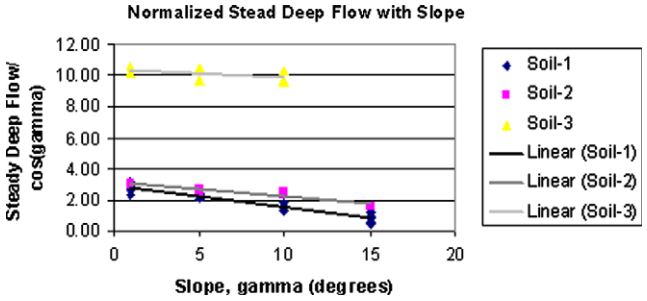

Fig. 4. Variation of normalized steady deep flow with slope.

reference rainfall rate for each slope tested. Initial conditions were designated using hydrostatic pressure head.

Brooks and Corey parameterization of soil hydraulic properties

Similar to Dagan and Bresler (1983), the Brooks and Corey model was used to describe soil properties for unsaturated flow. The soil water characteristic curve and the conductivity relationship take the form of a power-law to relate saturation, pressure head and conductivity,

$$\frac{K(\Psi)}{K_s} = \begin{cases} \left(\frac{\Psi_b}{\Psi}\right)^{2+3\lambda} = \left(\frac{\Psi_b}{\Psi}\right)^{n}; & n = 2+3\lambda;\ \Psi \leqslant \Psi_b \\ 1; & \Psi > \Psi_b \end{cases} \tag{1}$$

$$S = \begin{cases} \left(\frac{\theta-\theta_0}{\theta-\theta_0}\right) = \left(\frac{\Psi_b}{\Psi}\right)^{\lambda} \Rightarrow \frac{K(\theta)}{K_s} = S^{n/\lambda} = \left(\frac{\theta-\theta_0}{\theta-\theta_0}\right)^{n/\lambda}; & \Psi \leqslant \Psi_b \\ 1; & \Psi > \Psi_b \end{cases} \tag{2}$$

where $K(\Psi)$ is the hydraulic conductivity that is a function of the pressure head, Ψ, and depends on the saturated hydraulic conductivity K_s, air entry capillary pressure head, Ψ_b, and the pore size distribution index, λ. Here, θ is the volumetric water content, and θ_s and θ_0 are the saturated and residual water contents, respectively. When $\Psi \geqslant \Psi_b$, the hydraulic conductivity is equal to the saturated hydraulic conductivity, K_s. The Brooks and Corey relationships allow for the hydraulic conductivity to be related to water content through $K(\theta)$. Hysteresis was neglected, and Eqs. (1) and (2) were treated as single-valued functions.

Saturated–unsaturated equation for sloping surfaces

Combining the momentum (Darcy–Buckingham law) and continuity equation and rearranging in terms of pressure head results in the general saturated–unsaturated flow equation for 1-D flow perpendicular to the slope

$$C(\psi)\frac{\partial\psi}{\partial t} - \frac{\partial}{\partial z^*}\left[K(\psi)\frac{\partial\psi}{\partial z^*} - K(\psi)\cos\gamma\right] = 0 \tag{3}$$

where $C(\psi) = S_s + \frac{\partial\theta}{\partial\psi}$, S_s relates to the specific storativity of the soil. A centered implicit finite-difference model was developed for the numerical solution of Eq. (3). The model utilizes a Newton–Raphson iterative procedure for solving the system of nonlinear equations at each time step. The code developed by Govindaraju and Kavvas (1993) was modified for this study to handle arbitrary initial conditions and time-dependant boundary conditions.

With a rainfall application, a time-dependent boundary condition was imposed on the soil surface. The lower boundary was open to the atmosphere and was assigned a pressure head of zero. While impermeable sides exist, the Hydrus program demonstrated that the sides had very little effect, and a 1-D flow perpendicular to the soil surface would be a valid approximation. It was assumed that there is no lateral movement within the soil, and the impermeable sides would have no effect on the soil water movement. As described earlier, a short time passed between soil saturation and the beginning of each experiment and there was initially no bottom flux, so hydrostatic pressure distribution was prescribed as the initial pressure distribution.

Following Dagan and Bresler (1983), integrating the continuity equation from the soil surface to the front at $z^* = L_f$ yields:

$$q(L_f,t) - q(0,t) = -\frac{d}{dt}\int_0^{L_f}\{\theta(z^*,t) - \theta_i\}dz^* \tag{4}$$

where $q(z^*,t)$ is the Darcian flux, and L_f is the distance to the front, and θ_i is the uniform initial water content for the sharp-front model (Fig. 5). From the mean value theorem, the average value for q over the front depth, $\bar{q}$, is based on an average hydraulic conductivity, $\overline{K}$. Specifically, using the Brooks and Corey relationship in combination with Darcy's law and rearranging results in:

$$\bar{q}L_f = \cos\gamma\overline{K}L_f - \frac{\Psi_b}{1-n}\left[K(\theta_i)S_i^{-1/\lambda} - K(0,t)^{-1/\lambda}\right] \tag{5}$$

Eqs. (4) and (5) are the integrated forms of the continuity and momentum equations and do not represent any approximation.

Modified sharp-front model

From Eq. (4), the continuity equation for the sharp-front model (see Fig. 5) simplifies to

$$q(L^*,t) - q(0,t) = -\frac{d}{dt}\left[L^*(\bar{\theta}_t - \theta_i)\right];\quad L^* = L^*(t) \tag{6}$$

where L^* is the location of the equivalent front in the z^* direction, $q(L^*,t)$ is the Darcy flux in the z^* direction, $q(0,t)$ is the flow rate at the surface (infiltration), $\bar{\theta}_t$ is the time-varying uniform water content over $0 \leqslant z^* < L^*$, and θ_i is the initial water content. The cumulative infiltration depth into the soil is equivalent to the cumulative flux, $\forall_t$:

$$q(L^*,t) - q(0,t) = -\frac{d}{dt}(\forall_t);\quad \forall_t = L^*(\bar{\theta}_t - \theta_i) \tag{7}$$

Similarly, the integrated Darcy's law in Eq. (5) reduces to

$$\bar{q}L^* = \cos\gamma\overline{K}L^* - \frac{\Psi_b}{1-n}\left[K_iS_i^{-1/\lambda} - \overline{KS}^{-1/\lambda}\right] \tag{8}$$

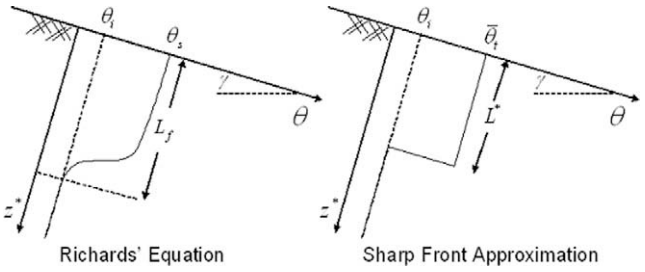

Fig. 5. Conceptualization of the spatial water content profile for the saturated–unsaturated flow equation and the sharp-front model at a given time.

where K_i is the initial hydraulic conductivity $K(\theta_i)$, S_i is the initial soil saturation, and $\overline{S}$ is time-varying uniform soil saturation. With the continuity equation and Darcy's Law for the sharp-front model, three surface boundary conditions are considered here to cover the entire range of conditions experienced in the laboratory experiments. These include (i) infiltration with constant water content, θ, at the soil surface, (ii) infiltration with a constant flux at the soil surface, and (iii) redistribution in the soil.

Infiltration with constant water content at the soil surface

In this scenario, it is assumed that there is a constant water content maintained at the soil surface. For a sharp-front model, surface values apply from the soil surface to the front. Substituting the water fluxes at the front and soil surface and the depth-averaged hydraulic conductivity into Eq. (6) and simplifying results in:

$$A_1 \cos\gamma + \frac{A_2}{L^*} = \frac{dl^*}{dt} \tag{9}$$

where

$$A_1 = -\frac{K_i - K_0}{\bar{\theta} - \theta}; \quad A_2 = -\frac{\Psi_b}{(1-n)(\bar{\theta} - \theta_i)}\left[K_i S_i^{-1/\lambda} - K_0 S_0^{-1/\lambda}\right]$$

Assuming $L^*(t=0) = 0$, and integrating results in:

$$T = \frac{L^*}{A_1 \cos\gamma} - \frac{A_2}{A_1^2 \cos^2\gamma} \ln\left[1 + \frac{L^* \cdot A_1 \cos\gamma}{A_2}\right] \tag{10}$$

where the first term is due to the gravitational flow and the second term is flow due to the suction forces at the front. The above integration can be carried out under the general initial conditions of $L^*(t) = L_i$.

Infiltration with constant flux at the soil surface

An alternate boundary condition at the soil surface is infiltration under prescribed flux conditions. If $q(0,t) = q_0 \cos\gamma$ is constant, then combining Eqs. (6) and (8) and simplifying further results in an implicit expression for $\overline{K}$, the average hydraulic conductivity applicable from the soil surface to the front

$$q_0 \cos\gamma = \overline{K}\cos\gamma - \frac{\Psi_b(\theta_s - \theta_0)}{(1-n)(q_0 - K_i)t\cos\gamma} \times \left[\frac{K_i S_i^{-1/\lambda}}{K_s^{\lambda/n}} \cdot \overline{K}^{\lambda/n} - \left(\frac{1}{K_s}\right)^{\frac{\lambda-1}{n}} \cdot \overline{K}^{\frac{n+\lambda-1}{n}} + \frac{S_i}{K_s^{-1/n}}\overline{K}^{\frac{n-1}{n}} - K_i S_i^{1-1/\lambda}\right] \tag{11}$$

Eq. (11) is an algebraic equation to be solved for $\overline{K}$. $\bar{\theta}$ is then obtained from Eqs. (1) and (2). Time to ponding, t_p, is obtained by setting $\overline{K} = K_s$ in Eq. (11), so that for $\theta_i = \theta_0$, $S_i = K_i = 0$, and $q_0 > K_i$.

$$t_p = -\frac{\Psi_b(\theta_s - \theta_0)(-K_s)}{(1-n)(q_0)(q_0 - K_s)\cos^2\gamma} \tag{12}$$

Eq. (11) is only valid for $t \leqslant t_p$. For $t > t_p$, the constant head boundary condition is used.

Redistribution

Let W be the amount (depth) of water that has infiltrated into the soil when rain ends, the continuity equation simplifies to Eq. (13). The amount W remains constant, but redistributes with time. We have

$$W = (\theta - \theta_i)L^* \tag{13}$$

In Eq. (13), θ is the current water content while θ_i is the initial water content and L^* is the perpendicular distance from the soil surface to the front. Using Darcy's law results in the following when the front is within the soil column

$$\frac{d\theta}{dt} = -\frac{(\theta - \theta_i)\cos\gamma}{W}K(\theta) \tag{14}$$

Eq. (14) is an ordinary differential equation that is easily solved numerically for $\theta(t)$ with $K(\theta)$ given by the Brooks–Corey relationship. The initial condition for θ in Eq. (14) is determined by knowing the soil water content when rain stops. The distance to the front is obtained from Eq. (13). The flux at the soil surface is zero, while at the bottom of the soil column it is $K(\theta_i)\cos\gamma$. Since θ_i is generally very small, the flux out of the soil column is essentially zero until the front reaches the plane.

After the front reaches the bottom of the soil column, the water does not redistribute but the water content keeps reducing as water leaves the soil column at the bottom. Darcy's law takes the form (Govindaraju and Kavvas, 1993)

$$K(\theta)\cos\gamma = -L_c\frac{d\theta}{dt} \tag{15}$$

where L_c is the length of the soil column. Using Eqs. (1) and (2), the solution is

$$\theta = \theta_0 + \{(\theta_b - \theta_0)^{1-n/\lambda} - \tilde{\alpha}(1 - \eta/\lambda)(t - t_b)\}^{\frac{1}{1-\eta/\lambda}} \tag{16}$$

where θ_b is the water content in the soil column when the front reaches the bottom of the column at time t_b and $\tilde{\alpha} = K_s\cos\gamma / L_c(\theta_s - \theta_0)^{n/\lambda}$. The water flux leaving the bottom of the column is again given by $K(\theta)\cos\gamma$. Thus there is a sudden discontinuity in the flux leaving the soil column at time t_b. Essig (2008) describes the extension to time-varying rainfall as well.

Surface flow and the kinematic approximation

Movement of water on the soil surface is modeled using the kinematic approximation (Singh, 1992)

$$q_x = \alpha\tilde{h}^m \tag{17}$$

where $\tilde{h}$ is the flow depth, q_x is the flow discharge per unit-width of the surface along the slope, and α and m are exponents. If Manning's equation is adopted, then $m = 5/3$ and $\alpha = c\sqrt{S_0}/n$ where S_0 is the surface slope, n is Manning's roughness coefficient, and c is a constant to account for units. For 1-D flow, the continuity equation is

$$\frac{\partial\tilde{h}}{\partial t} + \frac{\partial q_x}{\partial x} = r(t) \tag{18}$$

where r is the infiltration excess. The process of run-on (Morbidelli, et al., 2008) has not been incorporated as only homogenous soils with spatially uniform rainfall events were considered here. Eqs. (17) and (18) were solved numerically over each cell as a kinematic cascade. Surface flow was coupled to the numerical solution of both Richards' equation and the sharp-front model over sloped surfaces. These numerical solutions yielded surface and deep flow hydrographs, infiltration rates at the soil surface, as well as distributions of water content θ and pressure head Ψ in the subsurface region.

Comparisons of numerical results and observations

Effective saturated hydraulic conductivity

From previous studies (Philip, 1991; Chow et al., 1988), we expect the infiltration rate to vary as $\cos\gamma$ over sloping surfaces. In order to examine the behavior of saturated hydraulic conductivity, the relation between the observed steady deep flows and slope ($\sin\gamma$) from all experiments listed in Tables 2–4 was examined. Fig. 4 indicates that a linear relation would fit the data reasonably well. Extrapolating from this graph, Table 5 lists the saturated hydraulic conductivity for the three soils for zero slope.

Normalizing the observed steady deep flow with the theoretical steady deep flow ($K_s\cos\gamma$) using K_s values from Table 5, as shown in Fig. 6, still does not result in the expected horizontal straight line. The effect of slope was accounted for by the $\cos\gamma$ term, but the different non-zero slopes for the different soils on the graph suggest that a further correction is needed to account for different soils. The observed flow data do not vary with $K_s\cos\gamma$, but rather an "effective hydraulic conductivity", $\tilde{K}_s$, defined as follows:

$$\tilde{K}_s = K_s[1 - a\cdot\sin\gamma] \tag{19}$$

where K_s is obtained for a zero slope (Table 5). The effective saturated hydraulic conductivity, $\tilde{K}_s$, incorporates all the experimental variations observed in the results. Studies have known that the values of K_s obtained from standard infiltrometer studies are rarely reflective of field conditions. Rawls et al. (1993) for instance, suggested an effective conductivity of $K_s/2$ for field applications. Eq. (19) is formulated on the belief that $\tilde{K}_s$ is influenced by both the slope ($\sin\gamma$) and the soil type through a correction factor a, as suggested by Fig. 6.

A statistical test using the sampling theory of regression was conducted to confirm that the linear slope fits in Fig. 6 are significantly different from zero, suggesting that the correction factor in Equation (19) is necessary. The 95% confidence limits for the regression coefficient (slope of the normalized steady deep flow) were found to be significantly different from zero.

Table 5 shows the value of a in (19) for the three soils. Fig. 7 shows the normalized steady deep flow, normalized by $\tilde{K}_s\cos\gamma$ versus $\sin\gamma$. As expected, all three soils are centered on a one-to-one ratio of observed steady deep flows to a theoretical steady deep flow of $\tilde{K}_s\cos\gamma$. It may be observed that while data for Soil-2 and Soil-3 lie very close to the expected horizontal line, data for Soil-1 exhibit a greater spread as slope increases. Soil-1 is similar to a clayey soil with finer pores, but with a greater spread in pore sizes. Soil-3 is representative of a soil with a narrower distribution of pore sizes centered about larger pores. It is concluded that the soil pore size distribution plays a very prominent role in determining the $\tilde{K}_s$ and hence the dependence on soil type through the parameter a in (19).

Table 5
Parameters for the Brooks–Corey model to describe the hydraulic properties of the three soils.

	Soil-1	Soil-2	Soil-3
Hydraulic conductivity, K_s (mm/h)	2.93	3.20	10.37
Correction factor, a	−2.86	−1.90	−0.32
Saturated water content, θ_s	0.407	0.472	0.485
Residual water content, θ_r	0.034	0.041	0.043
Air entry pressure head, Ψ_b (mm)	−330	−250	−200
Lambda, λ	0.35	0.20	0.10
Specific storativity, S_s	0.00002	0.00003	0.00003

The rationale behind an effective saturated conductivity $\tilde{K}_s$ (Eq. (19)) is as follows. Infiltration tests are typically conducted under conditions where there is no horizontal water movement, and all the water moves essentially downward. In fact, infiltration tests with double ring infiltrometers, Guelph permeameters, and CSIRO's disc permeameters yielded saturated hydraulic conductivities that were one to two orders of magnitude greater than those indicated in Table 5.

When water moves on an infiltrating surface in response to slope it is postulated that two phenomena will act in conjunction to effectively alter the hydrodynamics of soil water. Firstly, water moving on the soil surface will exert a small pull on infiltrating water by applying an upward suction force that is proportional to $V^2/2g$, where V is the average surface water velocity which is several orders of magnitude larger than the pore water velocity. Thus, the small pore water velocity is likely to be reduced even by the small upward pull of $V^2/2g$. Further, it may be observed that V^2 is proportional to the slope, $\sin\gamma$, according to typical friction relationships (Manning's equation or Chezy's law). This explains the linear relationship between $\tilde{K}_s$ and $\sin\gamma$ in Fig. 6 and the formulation in Eq. (19). If there is the existence of this upward pull, then the hydrostatic assumption employed for most surface water equations over infiltrating surfaces is not valid. Nevertheless, Fig. 9 does show a non-negligible influence of slope.

Fig. 6 suggests that a second factor, depending on soil type, must also be playing a role since the effect is clearly different for the three soils. This second factor is hypothesized as being the pore size distribution which is known to play a key role in soil physics. For simplicity, a single large pore may be considered first. For a given set of upstream conditions of flow depth and velocity, the momentum will be such that all the water will enter a large pore and the amount of infiltrated water is less affected by given upstream conditions. As the pore diameter becomes smaller, the momentum of water on the surface will be such that part of it will "jump" across the opening allowing only a part of the upstream flux to "infiltrate" into the soil. Thus, soils with finer pores (such as Soil-1) are likely to be more affected by surface water velocity as observed in Fig. 6. It may be noted that this effect is solely due to the presence of a momentum component that is normal

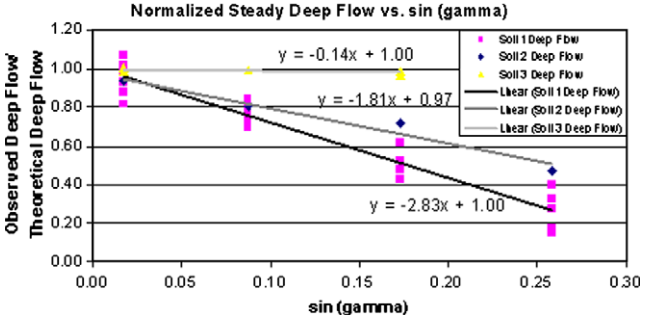

Fig. 6. Ratio of observed and theoretical deep flows versus slope.

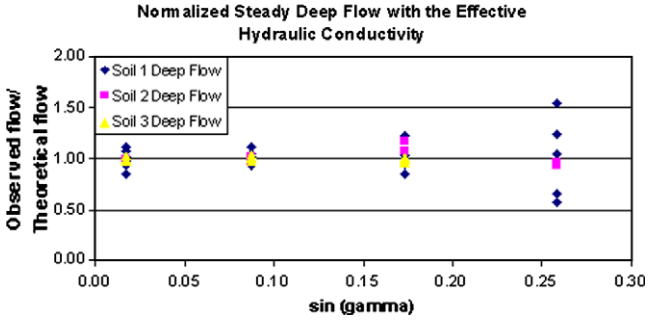

Fig. 7. Behavior of ratio of observed and theoretical flow after incorporating the correction factor for slopes and soil type.

to the direction of infiltrating water, and thus would not be manifested in infiltrometer experiments. The parameter a in Eq. (19) represents this effect.

These two factors may explain why surface runoff is observed over hillslopes even when the rainfall intensity is less than the saturated hydraulic conductivity as determined from in situ infiltrometer experiments. Two other factors that may affect infiltration include anisotropy and surface sealing. While the soil box was packed as carefully as possible specifically to avoid anisotropy, it is impossible to confirm uniform hydraulic conductivities within the soil column once the box is packed. Surface sealing may also affect the infiltration rate of the soil because it may also induce layering at the soil surface.

Hydraulic properties and parameter estimation results

In order to use the three numerical models, the input hydraulic parameters must be defined. The effective hydraulic conductivity was described in the previous section. The saturated and residual water contents were estimated during the laboratory experiments (see Table 5). However, Ψ_b, λ and S_s were estimated by matching the saturated–unsaturated equation solution to the experimental results for the lowest rainfall rate at the 1° slope. For Soil-2, this was experiment 1 in Table 3. Matching the hydrostatic distribution to the initial water content was first considered, then the deep flow, and finally the surface flow. Using Eqs. (1) and (2), the initial water content distribution was obtained. As shown in Fig. 8a, the initial water content distribution for Soil-2 matches observations at most depths, with the exception of sensor 5 at the 10 cm depth. The initial water content is the saturated value between the 67 and 45 cm depths and reduces at higher elevations. The initial distribution provides an estimate of Ψ_b for this soil (−250 mm for Soil-2).

For the sharp-front model, the initial water content distribution was assigned a saturated water content below the capillary fringe and an averaged water content above the capillary fringe as indicated in Fig. 8a to replicate hydrostatic conditions. The average water content above the capillary fringe for the sharp-front model was chosen so as to have the same initial soil water storage in the profile. The sharp-front infiltration calculations are based on the effective soil column length above the capillary fringe, the algebraic sum of the soil column length (67 cm) and the air entry pressure head (−25 cm for Soil-2). Deep flow is not initiated until the front reaches the depth of the effective soil column length, i.e. the top of the capillary fringe. Fig. 8b shows the deep flow hydrograph and Fig. 8c shows the surface flow hydrograph for experiment 1 in Table 3. Overall, by estimating the three parameters, Ψ_b, λ and S_s, a reasonable match was found between the saturated–unsaturated equation solution and experimental results for Soil-2. Fig. 8a–c shows results for the sharp-front model using the parameters estimated for the saturated–unsaturated flow model, i.e. no fitting experiments were carried out for the sharp-front model

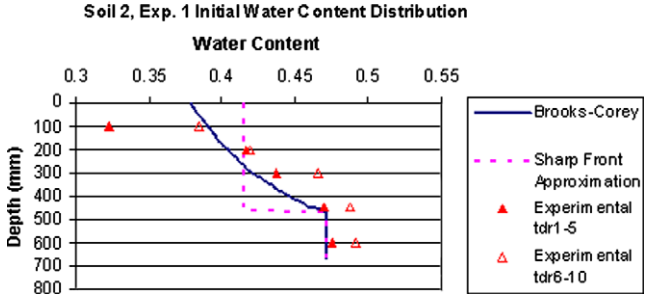

Fig. 8a. Observed and modeled initial water contents for Soil-2.

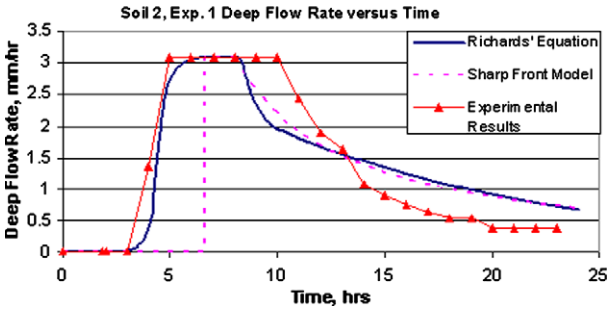

Fig. 8b. Fitted Soil-2 results for deep flow.

Observed soil water content distributions were not available for Soil-1 and Soil-3 experiments. As with Soil-2, the deep flow and surface flow results of saturated–unsaturated equation solution for Soil-1 and Soil-2 were matched to the experimental results at the lowest rainfall rate with 1° slope. Experiment 15 of Soil-1 in Table 2 and experiment 13 of Soil-3 in Table 4 were used for this purpose (Essig, 2008). Similar to Soil-2, more emphasis was given to matching the deep flow results than the surface flow values. In general, experimental results were better reproduced for Soil-3 by the saturated–unsaturated flow model. There are significant discrepancies between the saturated–unsaturated equation and sharp-front models, especially for deep flow results. These discrepancies are discussed later along with validation results. Table 5 summarizes the parameters for the three soils.

Hydrus simulations

Hydrus was selected to examine the subsurface pressure heads and flow patters in a qualitative manner only. Fig. 9 shows the water content distribution at selected times during the simulation for the highest rainfall rate at the 15° slope for Soil-1 i.e. the most critical case. As shown in the figure, the soil is saturated at the surface by 1 h, but a band of unsaturated zone exists in the middle of the soil column. The contours are curved at the impervious edges, but the flow is essentially 1-D over most of the profile. By 2 h, the soil is completely saturated, and remains so until 8 h when the rainfall stops. The drainage pattern is revealed more strongly at 10 h where one can see that the 15° slope shows more curvature in water content contours at the impermeable soil box edges, but flow is primarily moving in a 1-D fashion perpendicular to the soil surface. This 1-D flow pattern is essentially maintained for 24 h. These results do not indicate the development of a seepage face.

The uniform nature of the water content perpendicular to the slope (Fig. 9) indicates that return flow is not likely. Hydrus results for the other slopes and soils support the findings of the Soil-1 experiment at 15° slopes for a 20 mm/h rainfall rate (Essig, 2008).

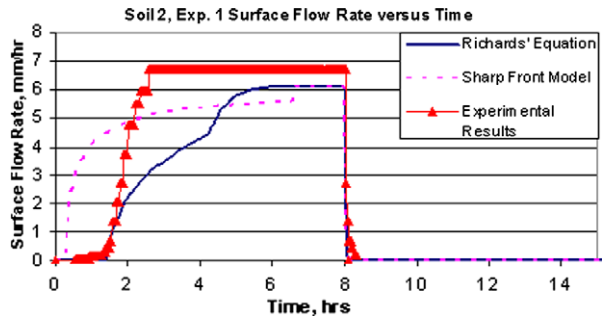

Fig. 8c. Fitted Soil-2 results for surface flow.

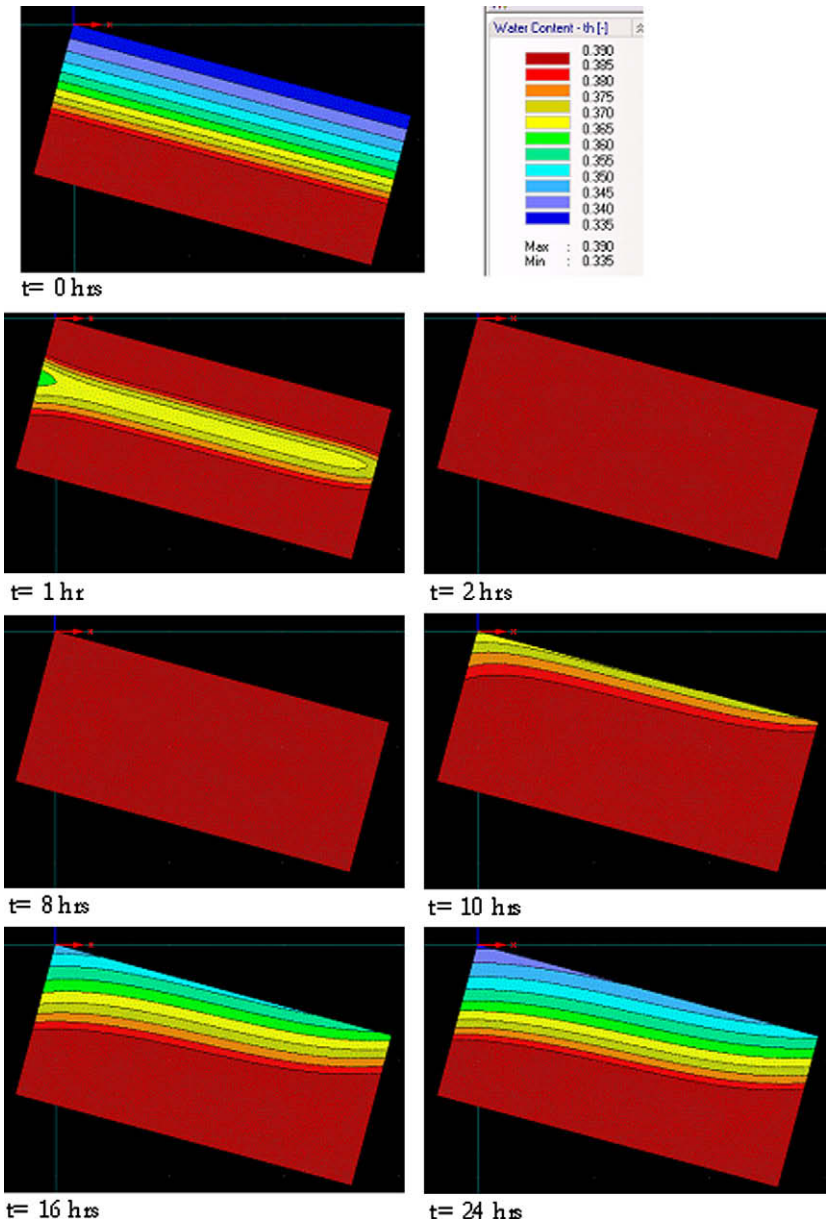

Fig. 9. Simulated water content contours at different times using the Hydrus model for Soil-1 under a 15° slope and 20 mm/h rainfall rate.

Saturated–unsaturated equation and sharp-front model results

Deep flow and surface flow were collected for the duration of all soil experiments. Soil water contents at various locations were also collected for Soil-2 experiments. Fig. 10 shows the deep flow hydrographs at the 10 mm/h reference rainfall for Soil-1. The saturated–unsaturated equation numerical solution performed very well for most slopes. However, the peak flowrate for the 15° slope was higher than the experimental data. This may be because observed deep flows have very small magnitudes, and measurement errors are likely to be relatively larger in this range. Also for the 15° slope, the experimental data showed that deep flow started before that predicted by saturated–unsaturated equation. Perhaps the initial condition was wetter than indicated by a hydrostatic initial condition in this case.

Deep flow is not initiated in the sharp-front model unless the front reaches the top of the capillary fringe. This causes a systemic delay in onset of deep flow as shown in Fig. 10, with the discrepancy being particularly large for the 15° slope. If the front reaches the top of the capillary fringe before the rainfall duration of 8 h (1° and 5° slopes), then it is maintained at a steady rate until rain stops. During recession, the sharp-front solution predicts a slower receding hydrograph than either the observations or results from saturated–unsaturated equation. For the 10° and 15° slopes in Fig. 10, the rainfall rate is low enough that the front does not reach the top of the capillary fringe during rainfall (i.e. >8 h). In these cases, the deep flow hydrograph for the sharp-front model does not possess a flat peak, and immediately recedes from that time on. However, the recession limb is far more prolonged than indicated by observations.

The saturated–unsaturated equation model results for Soil-2 and Soil-3 match experimental data more closely than for Soil-1 as shown in Figs. 11 and 12, respectively. In Figs. 10–12, the saturated–unsaturated equation model is better for the milder slopes, perhaps because the 1-D approximation is more suitable for mild slopes. The sharp-front model results for Soil-2 are similar to Soil-1, even though there is an improved representation of the receding limb when compared to observations. The deep flow re-

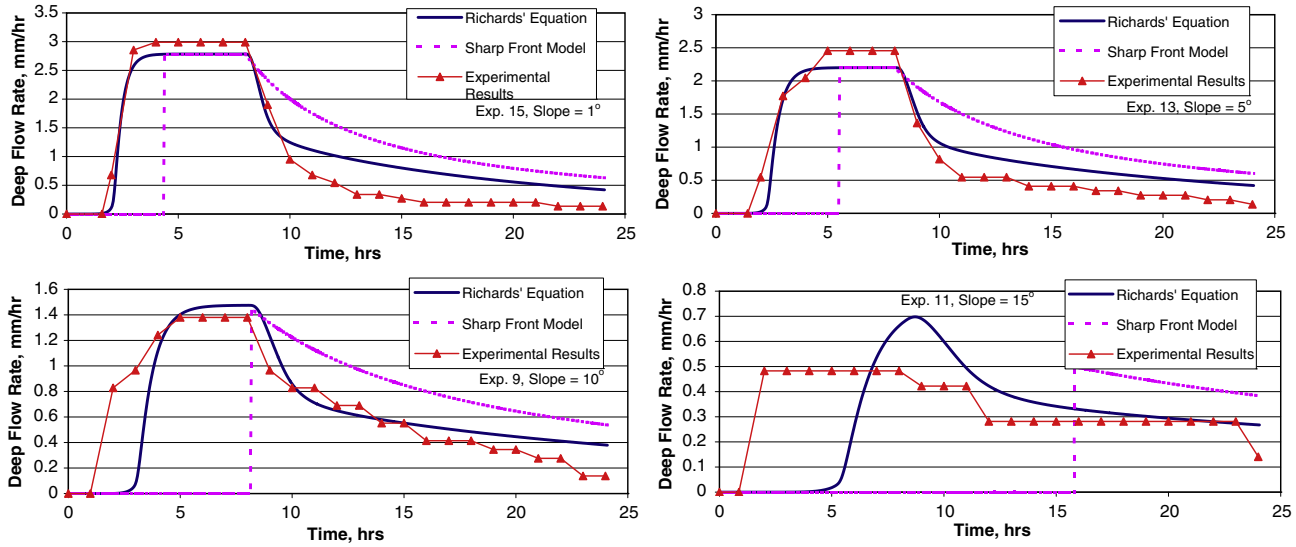

Fig. 10. Deep flow results for Soil-1under 10 mm/h reference rainfall.

sults for Soil-3 are quite encouraging for both models as all aspects of the observed hydrograph are replicated well. The better performance of the sharp-front model for Soil-3 is expected because it is a coarse grained soil where the sharp-front approximation is more appropriate.

Representative cases of surface flow hydrographs include 10 mm/h reference rainfall for Soil-1 in Fig. 13 and 10 mm/h reference rainfall for Soil-2 in Fig. 14, and 20 mm/h reference rainfall for Soil-3 in Fig. 15. In Fig. 13, the rising limb of the sharp-front model exhibits a sudden jump in the 1° and 5° slopes. This occurs because as soon as the front reaches the top of the capillary fringe, the infiltration model changes. The front is not allowed to grow any further, according to Eq. (9), and the infiltration rate is equal to $\tilde{K}_s \cos\gamma$. This abrupt reduction in infiltration rate causes a corresponding rise in surface flow.

Similar to results of deep flow hydrographs, the surface flow results for Soil-2 and Soil-3 match experimental data more closely than Soil-1 as shown in Figs. 14 and 15, respectively. Curiously, the rising limb of the observed hydrograph lies between the earlier sharp-front model hydrograph and that of the saturated–unsaturated equation results. A more gradual rise to peak is predicted by the saturated–unsaturated model, especially for Soil-2 in Fig. 14. The peak value of the observations is rarely reproduced accurately by either model, but this may be attributed to the variability in the estimation of $\tilde{K}_s$. Overall, the agreement between the deep and surface flow hydrographs from the two models to experimental results indicates that using an effective hydraulic conductivity is a reasonable approach to represent the influence of surface water movement on sloping surfaces.

It is also beneficial to see how water content behaves with time at various depths. The Soil-2 water content distributions at 10, 30 and 60 cm depths through time for the 1° slope at 10 mm/h reference rainfall are included in Fig. 16. The saturated–unsaturated equation and sharp-front model water contents matched the experimental water contents fairly closely at 10 and 30 cm depths. At the 60 cm depth, the saturated–unsaturated equation estimated water content closely, but the sharp-front model diverged from experimental results because the model calculates uniform water

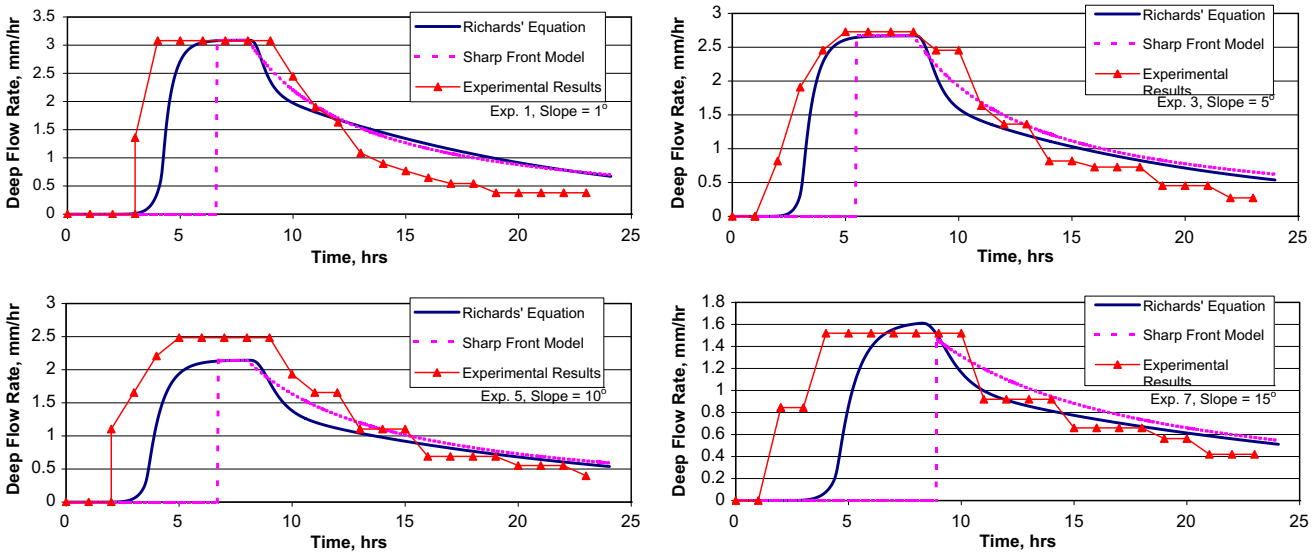

Fig. 11. Deep flow results for Soil-2 at 10 mm/h reference rainfall rate.

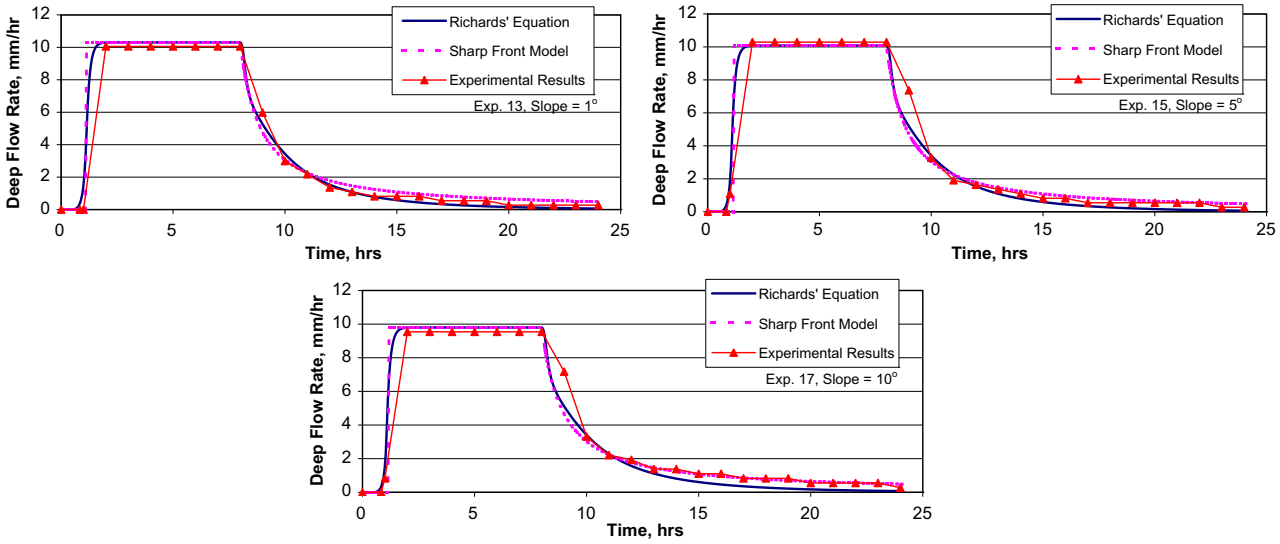

Fig. 12. Deep flow results for Soil-3 at 20 mm/h reference rainfall rate.

content throughout the front once it reaches the bottom of the soil column. The sharp-front model will be unable to match experimental results below the capillary fringe unless the entire soil column is saturated.

An interesting situation occurred for the sharp-front approximation at some of the steeper slopes for Soil-1 and Soil-2 if the front did not reach the capillary fringe at the time the rainfall stopped. To replicate experimental conditions, initial water content was maintained below the front until the redistribution front reached that elevation. At that time, the water content would reset to the redistribution front water content. This causes a small jump in the saturated water content. Redistribution was not a problem for the other Soil-1 10 mm/h reference rainfall slopes shown. The wetting fronts for all Soil-3 experiments reached the soil column bottom before rainfall ended. The wetting front did not reach the capillary fringe before rainfall ended for all Soil-1 and Soil-2 15° slopes and for some of the 10° slopes.

Summarizing remarks

This study was an effort at improving our understanding of infiltration and deep flow on sloping surfaces by comparing numerical model results to observations from controlled laboratory experiments. Out of numerous laboratory studies conducted at University of Perugia, Italy, three sets of experiments dealing with artificial rainfall on homogeneous soils were identified for this analysis. A preliminary analysis of the data indicated that increased slope had a positive influence on surface flow. Further, it was hypothesized that return flow of soil water may contribute to surface flow as the slope increased.

Three mathematical models were employed to understand and extrapolate from these experimental results. These models were: (i) the Hydrus numerical model, (ii) numerical solution of 1-D saturated–unsaturated flow on sloping surfaces, and (iii) a simplified 1-D sharp-front model for sloping surfaces. The Hydrus program was used only for a qualitative analysis to assess wall effects and

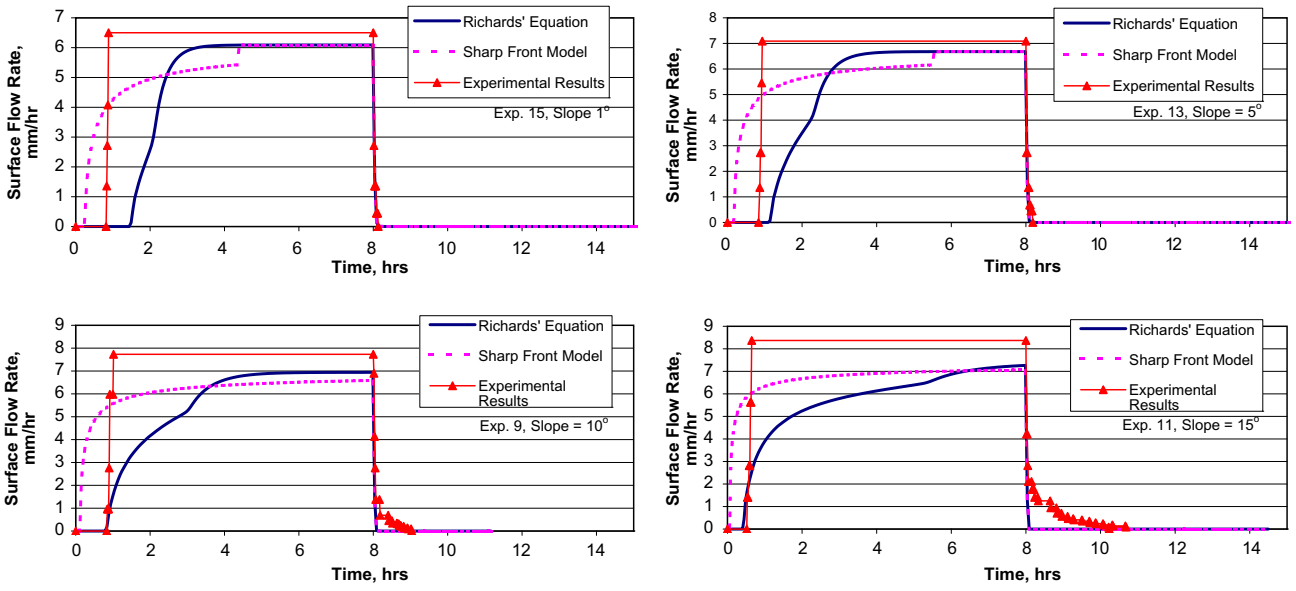

Fig. 13. Surface flow results for Soil-1 at 10 mm/h reference rainfall rate.

return flow. For the latter two models, a surface flow component based on the kinematic wave approximation for shallow flows was externally coupled to the subsurface flows to route water over the soil surface.

For each soil, one experiment at the lowest slope and rainfall rate was utilized for estimation of model parameters that could not be measured independently. The hydraulic conductivity for each soil was calculated by normalizing the observed deep flow with the slope, $\cos\gamma$. It was discovered that $\cos\gamma$ was not adequate to describe the variation in infiltration rate and deep flow. As slope increased, model results were found to diverge from experimental results. The following conclusions were drawn from this analysis:

- The simple correction, $\cos\gamma$, for sloping surfaces is not sufficient to account for slope effects in determining infiltration. An effective hydraulic conductivity, $\tilde{K}_s$, should be included to account for slope and soil type.
- The steady deep flow equals the effective hydraulic conductivity multiplied by the slope, $\tilde{K}_s \cos\gamma$.
- The steady surface flow equals $R_{eff} - \overline{K}_s \cos\gamma$. As shown by the surface flow figures, this adequately describes the experimental results.

On sloping surfaces, an effective saturated hydraulic conductivity is required to account for decreased infiltration with increasing slopes. The pore size distribution of the soil plays an important role in determining the influence of slope and moving water on infiltration process.

A new sharp-front model was also developed to supplement the numerical solutions. As indicated by Dagan and Bresler (1983) and Govindaraju et al. (1992), the sharp-front model is expected to perform well at the field scale, where heterogeneity in soil properties dominates average behavior and local model errors are cancelled out during the averaging process. In this study, the sharp-front model was utilized for single realizations, and further, no parame-

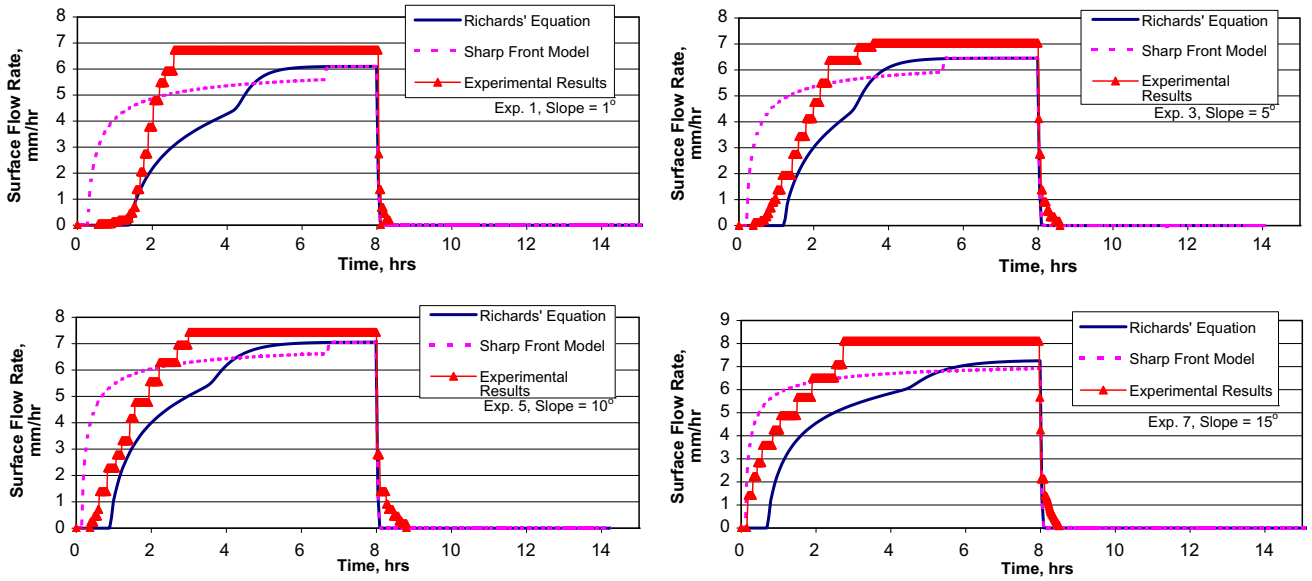

Fig. 14. Surface flow results for Soil-2 under 10 mm/h reference rainfall rate.

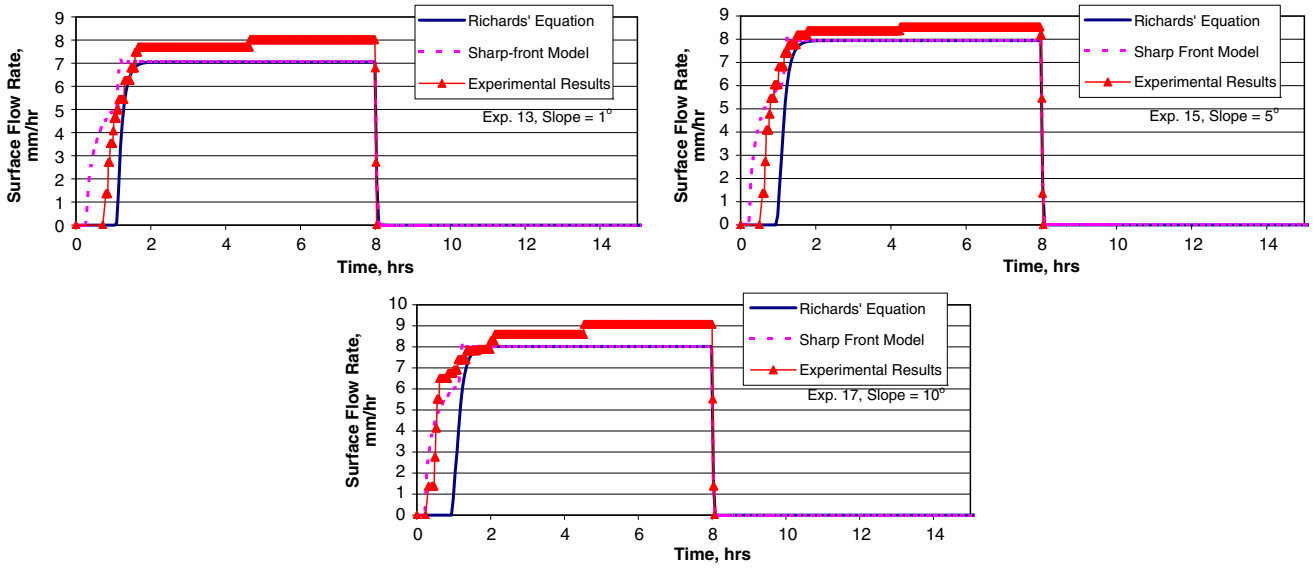

Fig. 15. Surface flow results for Soil-3 under 20 mm/h reference rainfall rate.

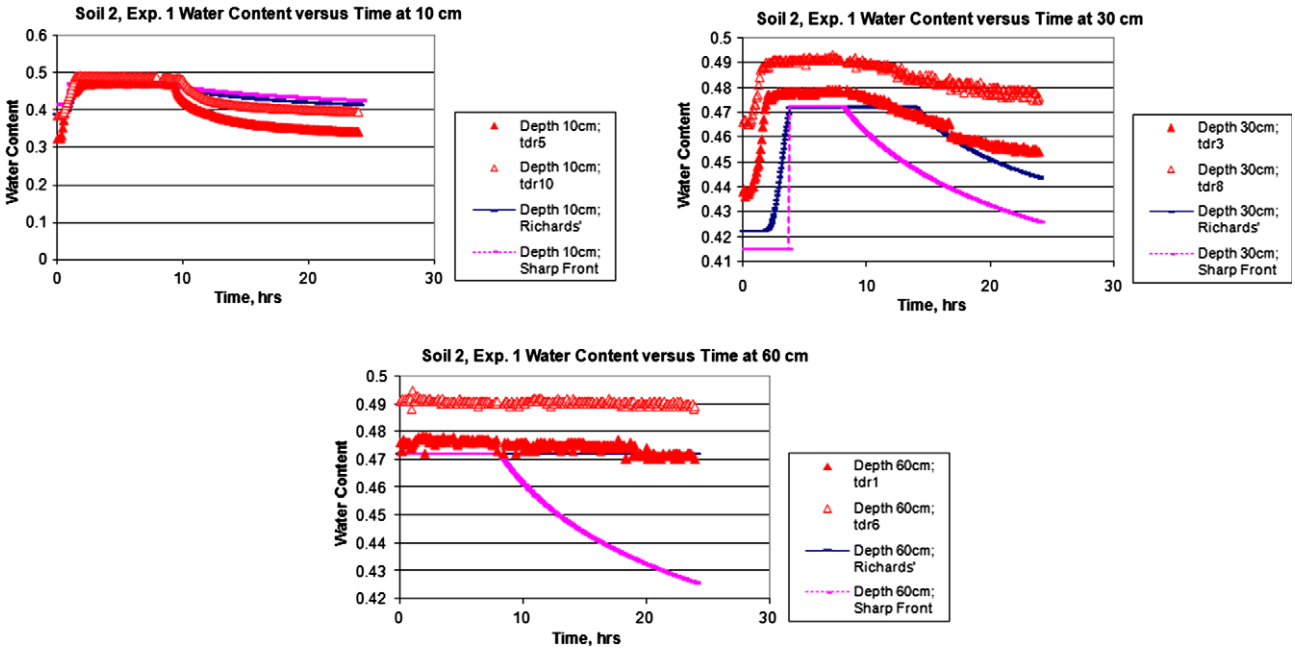

Fig. 16. Observed and simulated water content versus time at different depths for Soil-2 under 1° surface slope.

ter estimation was conducted explicitly for this model. Nevertheless, the sharp-front model was shown to perform well for coarser soils (Soil-3) where model assumptions are better met. The sharp-front model was better for simulating surface flow hydrographs than for the deep flow hydrographs. The deep flow hydrographs were particularly off when the front did not reach the top of the capillary fringe before rainfall stopped. Another challenge for the sharp-front model was posed by the hydrostatic initial conditions with a capillary fringe and the requirement of a constant atmospheric pressure head at the bottom – neither of which were represented by the sharp-front model. Thus, even though the sharp-front model is very attractive in terms of simplicity and insight it provides (analytical expressions for infiltration rate, deep flows, time to ponding, etc.), its applicability is limited to coarser soils and more care must be exercised when adopting this simpler model.

References

Chen, L., Young, M.H., 2006. Green–Ampt infiltration model for sloping surfaces. Water Resources Research 42, W07420. doi:10.1029/2005WR004468.

Chow, V.T., Maidment, D.R., Mays, L.W., 1988. Applied Hydrology. McGraw-Hill, pp. 99–122.

Dagan, G., Bresler, E., 1983. Unsaturated flow in spatially variable fields 1. Derivation of models of infiltration and redistribution. Water Resources Research 19 (2), 413–420.

Essig, E.T., 2008. Modeling infiltration and deep flow over sloping surfaces, M.S. Thesis, Purdue University, 268 p.

Govindaraju, R.S., Kavvas, M.L., 1993. Development of an approximate model for unsaturated flow with root water uptake under rectangular water content profiles assumption. Journal of Hydrology 146, 321–339.

Govindaraju, R.S., Or, D., Kavvas, M.L., Rolston, D.E., Bigger, J.W., 1992. Error analyses of simplified unsaturated flow models under large uncertainty in hydraulic properties. Water Resources Research 28 (11), 2913–2924.

Govindaraju, R.S., Kavvas, M.L., Jones, S.E., Rolston, D.E., 1996. Use of Green–Ampt model for analyzing one-dimensional convective transport in unsaturated soils. Journal of Hydrology 178, 337–350.

Green, W.H., Ampt, G.A., 1911. Studies in soil physics. 1. The flow of air and water through soils. Journal of Agricultural Science 4 (1), 1–24.

Mein, R.G., Larson, C.L., 1973. Modeling infiltration during a steady rain. Water Resources Research 9 (2), 384–394.

Morbidelli, R., Corradini, C., Saltalippi, C., Govindaraju, R.S., 2008. Laboratory experimental investigation of infiltration by the run-on process. ASCE Journal of Hydrologic Engineering 13 (12), 1187–1192.

Philip, J.R., 1991. Hillslope infiltration: planar slopes. Water Resources Research 27 (1), 109–117.

Poesen, J., 1984. The influence of slope angle on infiltration rate and hortonian overland flow volume. Zeitschrift Fur Geomorphologie 49, 117–131.

Rawls, W.J., Ahuja, L.R., Brakensiek, D.L., Shirmohammadi, A., 1993. Infiltration and soil water movement. In: Maidment, D.R. (Ed.), Handbook of Hydrology. McGraw-Hill, Inc., New York, pp. 5.1–5.51.

Simunek, J., Sejna, M., van Genuchten, M.Th., 2007. User Manual, The Hydrus Software Package for Simulating the Two- and Three-Dimensional Movement of Water, Heat, and Multiple Solutes in Variably-Saturated Media, Prague, Czech Republic: PC-Progress, pp. 45–48.

Simunek, J., Sejna, M., van Genuchten, M.Th., 2007. Technical Manual, The Hydrus Software Package for Simulating the Two- and Three-Dimensional Movement of Water, Heat, and Multiple Solutes in Variably-Saturated Media, Prague, Czech Republic: PC-Progress, pp. 1–8.

Singh, V.P., 1992. Elementary Hydrology. Prentice-Hall, Inc., Englewood Cliffs, NJ, pp. 203–216.

Smith, R.E., Woolhiser, D.A., 1971. Overland flow on an infiltrating surface. Water Resources Research 7 (4), 899–913.